

Integrative Modeling and Engineering of ZnO Grain Boundaries: A Pathway to Enhanced Thermoelectric Performance

Gbadebo Taofeek Yusuf¹, Sukhwinder Singh², Alexandros Askounis¹, Zlatka Stoeva³ and Fidine Tchuenu-Magaia^{1*}

¹ Energy and Green Technology Research Group, Centre for Engineering Innovation and Research, University of Wolverhampton, Telford Innovation Campus, Telford TF2 9NT, UK

² Magnetics and Materials Research Group, School of Engineering, Cardiff University, Cardiff, UK, CF24 3AA

³DZP Technologies Limited, Cambridge CB4 2HY, United Kingdom

Contact: F.Tchuenu-Magaia@wlv.ac.uk

Abstract

Achieving higher performance in zinc oxide (ZnO) at room and mid-temperatures is a topic of considerable interest, particularly for applications where energy conversion efficiency is crucial. This study focuses on grain boundary engineering techniques and an innovative modeling approach to optimize the thermoelectric properties of ZnO materials for improved performance. An analysis was conducted to investigate the influence of grain boundaries on ZnO materials and to evaluate the performance outlook of ZnO at mid-temperatures using the quality factor B as a descriptor. The findings indicate that the thermoelectric performance of ZnO could be significantly enhanced at low and mid-range temperatures if polycrystalline samples with engineered grain boundaries achieve low lattice thermal conductivity. Consequently, an integrative model was developed to analytically examine the impact of the barrier height (Φ_{GB}), the mean free path (l) of carriers, and the effective mass of carriers on the carrier charge mobility. The simulation results show that reducing Φ_{GB} from 0.5 eV to 0.1 eV resulted in a 45% increase in electron mobility, thereby facilitating the overcoming of energy barriers that impede charge transport. Furthermore, an increase in the mean free path from 5 nm to 25 nm significantly increased charge carrier mobility, indicative of fewer scattering events and the maintenance of higher velocities over prolonged distances. The study also shows that as the effective mass increases from 0.8 to 1.0, electron mobility increases, peaking at $1.0 m_e^*$ which suggests an optimal balance of effective mass where electron mobility is maximized, implying an intricate interplay between carrier mass and lattice interaction forces within the material. Drawing on these insights, a range of strategies aimed at improving the figure of merit was proposed. These strategies include microstructural engineering, advanced doping techniques, and passivation of grain boundaries. These findings provide a systematic approach to grain boundary engineering that could potentially transform ZnO into efficient materials for thermoelectric applications. Moreover, this research lays a foundational framework for further empirical validation and development of ZnO-based thermoelectric materials, aiming for enhanced performance and sustainability in energy harvesting technologies.

Keywords: Grain boundary, Mobility, Thermoelectricity, ZnO, Quality factor

1. Introduction

Thermoelectricity has attracted significant attention due to its potential in waste heat recovery and solid-state refrigeration applications^{1,2}. However, traditional thermoelectric materials such as bismuth and lead telluride face challenges such as high cost, toxicity, and limited efficiency³. Doped ZnO emerges as a promising alternative as it offers advantages such as abundance, low cost, and environmental friendliness, making it an attractive candidate for thermoelectric applications⁴. Furthermore, ZnO exhibits tunable electrical properties and, a high Seebeck coefficient, and has the potential for achieving low thermal conductivity with doping, which are essential characteristics for efficient thermoelectric materials⁵⁻⁹. However, achieving a high figure of merit

(ZT) at a low or mid-temperature range presents a primary challenge¹⁰. These limitations arise from intrinsic properties such as strong ionic bonds, which inherently reduce electrical conductivity and contribute to high thermal conductivity¹¹. Grain boundary engineering is a promising method to enhance the performance of ZnO thermoelectric materials^{12–16} as it is realistic to optimize the thermoelectric properties by manipulating the microstructure at grain boundaries^{17–19}.

Several studies have demonstrated the potential of grain boundaries in modifying the thermal and electrical transport properties of materials such as NbFeSb half-Heusler alloys²⁰, SrTiO₃^{17,21,22}, SnSe films²³, and Bi₂Te²⁴. For example, the introduction of boron has been found to facilitate grain boundary engineering in Bi₂Te₃-based alloys, resulting in improved thermoelectric and mechanical properties¹⁸. Additionally, in PbTe nanocomposites, grain-boundary potential barrier scattering has been identified as the primary scattering mechanism affecting the Seebeck coefficient²⁵. While grain boundaries can enhance thermoelectric properties, they can also impede electronic performance in Mg₃Sb₂^{26,27} and SrTiO₃^{17,22}. Therefore, a deeper understanding of the influence of grain boundaries on thermoelectric transport and its properties is crucial for optimizing the efficiency of materials^{16,23,26}. Existing studies have explored grain boundaries in various materials and their general effects on material properties; however, there is a lack of detailed investigation specifically targeting ZnO. This gap is particularly critical given that precise control of grain boundary chemistry in ZnO is essential for achieving a higher ZT. The complex and variable microstructure of ZnO, which includes factors like the size, distribution, and specific properties of its grain boundaries, directly influences its thermoelectric performance^{27,28}. Effective management of these properties is necessary to optimize the trade-off between lattice thermal conductivity and electrical power factor, both of which are important in enhancing the material's thermoelectric efficiency.

This study established a path towards enhancing the electronic transport performance of ZnO by using integrative modeling to investigate how modifications to the grain boundary barrier height (Φ_{GB}), mean free path of charge carriers, and effective mass impact electron mobility. This work not only fills a crucial research gap but also sets the stage for future empirical and theoretical investigations to further refine and apply the findings within the field of energy harvesting materials.

2. Influence of grain boundaries on materials properties

Grain boundaries are interfaces that separate individual crystalline grains in poly-crystalline materials²⁹. These boundaries can originate from various factors, including atomic bonding, strain in the grain interior, and the presence of impurities or solutes^{29,30}. The existence of grain boundaries could significantly influence the physical, and mechanical properties of materials¹⁷. For instance, it can affect the electrical properties of ferroelectric materials³¹, the mechanical behavior of materials like copper³², and the thermal conductivity of nanocrystalline films³³. The grain boundaries can lead to phenomena such as grain boundary sliding, which affects the deformation behavior of material³⁴ and can act as barriers, influencing the movement of defects like dislocations and impacting the properties of materials³⁰. It can also significantly influence the microstructure and properties of ceramics like ZnO through mechanisms such as solid-state activated sintering and abnormal grain growth, as well as affecting electrical conductivities via space charge depletion layers and grain boundary resistivity³⁵. Hence, the need to study these effects arises to optimize the material performance.

However, in this research, the impact of grain boundaries on the thermoelectric properties of ZnO is analyzed by obtaining transport data such as electrical conductivity, Seebeck coefficient, and power factor from existing literature^{2,4,6–10,12–15,36–39}. This includes data for both single-crystal and polycrystalline forms of ZnO which were processed to compare the inherent scattering mechanisms in the two forms of ZnO to enable a detailed analysis of how grain boundaries act as scattering centers for charge carriers. Figure 1(a) shows the analysis of electrical conductivity across varying temperatures. It is observed that electrical conductivity for single-crystal decreases with rising temperature due to enhanced phonon scattering, which impedes charge carrier flow. However, polycrystalline samples exhibit a more pronounced decline in conductivity, indicating the presence of complex scattering mechanisms at the grain boundaries⁴⁰. At low temperatures, additional scattering centers introduced by grain boundaries increase electrical resistivity. However, these effects are less significant at higher temperatures as carriers gain sufficient energy to overcome these barriers⁴¹. Variability among polycrystalline samples can often be attributed to differences in grain size, boundary properties, and potential impurity phases that affect charge transport³⁷. Samples (Poly crystal 1 and crystal Poly 2) with higher conductivity might possess

fewer grain boundaries or have undergone treatments that reduce grain boundary defects. The influence of grain boundaries on the effective mass and mobility of charge carriers, as described by the effective mass and Drude models, suggests significant reductions in carrier mobility due to increased scattering events⁴². This effect is similar to observations in materials like Mg_3Sb_2 and $SrTiO_3$ and can be effectively conceptualized using a series circuit model, where grain and grain boundary phases are considered as resistances for the flow of charge carrier, with separate components impacting overall transport properties¹⁷.

Figure 1(b) shows the temperature dependence of the Seebeck coefficient. Polycrystalline samples demonstrate similar trends but at reduced magnitudes compared to single crystals. The presence of grain boundaries in polycrystalline materials likely disrupts charge flow, diminishing the magnitude of the Seebeck coefficient. The variations in the slopes among polycrystalline samples might relate to differences in microstructure, such as grain size and porosity, which impact how grain boundaries scatter charge carriers⁴³. The lower Seebeck coefficient in poly-crystalline materials indicates the potential for optimization of grain boundary characteristics to enhance thermoelectric efficiency.

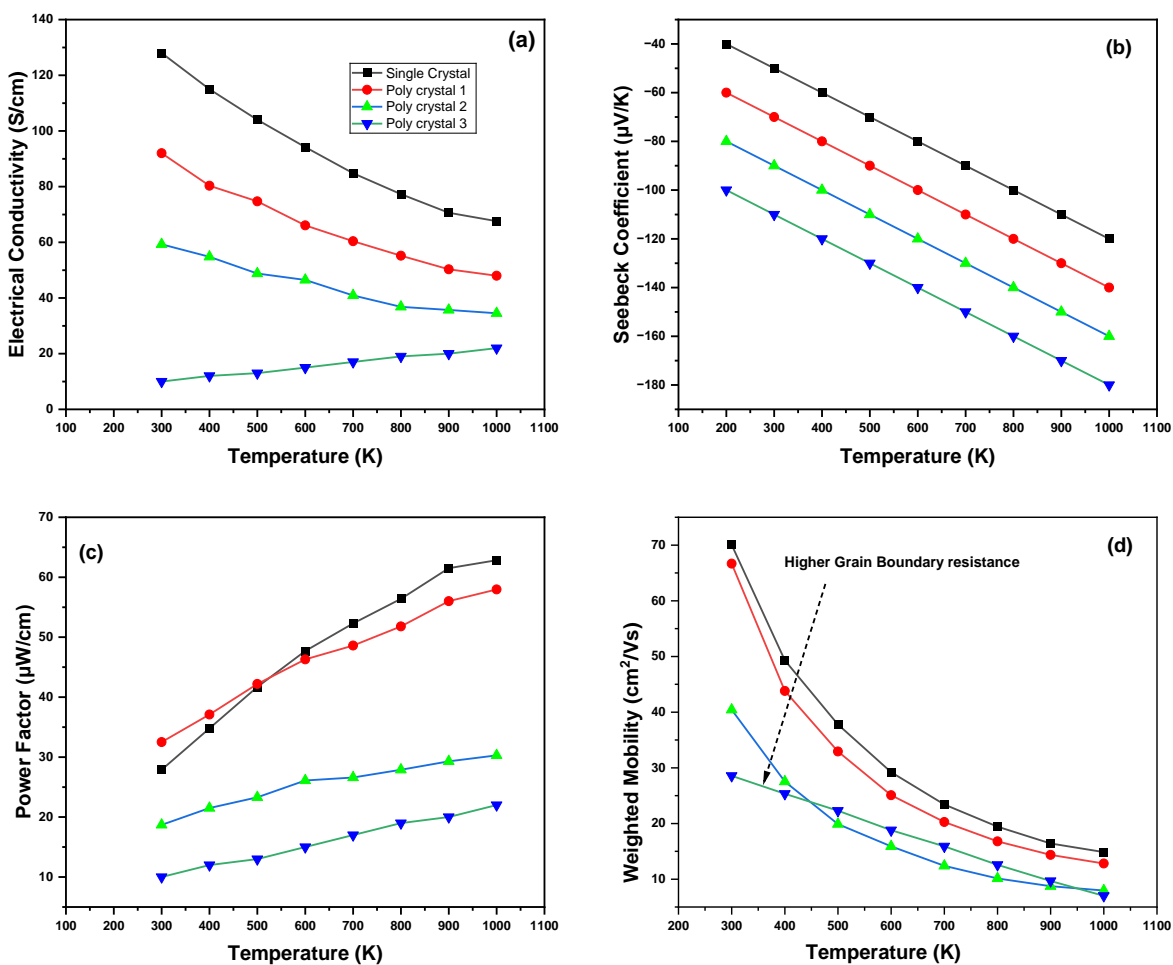


Figure 1 (a) Electrical conductivity (b) Seebeck coefficient for ZnO (c) Power factor (d) Weighted mobility of ZnO showing a distinct drop in polycrystalline samples at lower temperatures, which suggests significant grain boundary scattering effects, contrasting with the higher mobility maintained by single crystals across the range 2,4,6-10,12-15,36-39

Weighted mobility provides a method for conducting an in-depth analysis of the inherent electronic transport properties of thermoelectric materials. It offers similar information as Hall resistivity measurements, utilizing Seebeck coefficient and Electrical conductivity data. Figure 1(d) shows the trend of decreasing weighted

mobility with increasing temperature which is evident across all ZnO samples. The primary scattering mechanisms were analyzed using a weighted mobility (μ_w) calculation⁴⁴ derived from equation (1):

$$\mu_w = \frac{3h^2\sigma}{8\pi e(2m_0k_{\beta}T)^{3/2}} \left[\frac{\exp\left(\frac{ISI}{k_{\beta/e}} - 2\right)}{1 + \exp\left[-5\left(\frac{ISI}{k_{\beta/e}} - 1\right)\right]} + \frac{\frac{3}{\pi^2} \frac{ISI}{k_{\beta/e}}}{1 + \exp\left[5\left(\frac{ISI}{k_{\beta/e}} - 1\right)\right]} \right] \quad (1)$$

This equation considers diverse scattering processes affecting charge carrier mobility and offers insights into the transport behavior in thermoelectric materials.

Single crystals maintain high electron mobility across various temperatures, indicating minimal scattering effects. In contrast, polycrystalline samples experience a decrease in mobility at lower temperatures due to the existence of grain boundaries, which in turn results in the manifestation of complex scattering mechanisms. However, as the temperature rises, the impact of grain boundary scattering is minimal compared to phonon-related scattering, leading to a convergence in mobility levels between polycrystalline and single-crystal samples at higher temperatures. This behavior shows the importance of developing specific thermoelectric design strategies that enhance performance across different temperature regimes, aiming to improve low-temperature functionality while preserving efficiency at high temperatures⁴⁶. In the case of polycrystalline ZnO samples, the existence of grain boundaries presents an advantageous opportunity to employ the phonon-glass electron-crystal (PGEC) strategy, thereby enhancing ZT⁴⁵.

The PGEC strategy is crucial as it seeks to design materials that minimize lattice thermal conductivity without adversely affecting the electrical conductivity⁴⁵. This balance is essential for achieving high thermoelectric efficiency and can be achieved by developing ZnO samples with smaller grain sizes or by creating a large number of grain boundaries⁴⁶. However, a major drawback of this approach is that as thermal conductivity decreases, electron scattering also increases, which could potentially lead to a reduction in the power factor or weighted mobility⁴⁷. In this context, an integrative model that incorporates the mean free path of charge carriers, effective mass, and potential height barrier at grain boundaries is developed to allow for a comprehensive understanding of how microstructural features influence both electron and phonon transport. This model is necessary as it helps in quantifying the trade-offs between reducing phonon transport and maintaining or enhancing electron mobility within the material.

Furthermore, the model will offer significant insights into optimizing the thermoelectric properties of ZnO by highlighting the specific roles of various microstructural characteristics. For example, the potential height barrier at grain boundaries can be tailored to optimize carrier filtering effects that enhance electrical conductivity while suppressing undesirable phonon conductivity. Similarly, understanding the effective mass and mean free path helps in tuning the electronic band structure and scattering mechanisms, respectively, to maximize the power factor. Therefore, this model is not only a tool for theoretical analysis but also serves as a guide for experimental and practical applications.

3. Integrative Model development

The integrative model was developed to predict and optimize the thermoelectric performance by accounting for not only the grain boundary parameters, Φ_{GB} ; effective mass (m_*) but also the mean free path of charge carriers (l). It is an integrative approach combining several physical principles as shown in (3).

$$\mu_w = n\sigma \left(\frac{m_*}{m_e}\right)^{3/2} \exp\left(-\frac{K_{\beta}T\Phi_{GB}}{e}\right) \left(1 - \frac{l}{w_{GB}}\right) \quad (2)$$

Where:

- n is the charge carrier concentration
- σ is the electrical conductivity
- m_* the charge carrier concentration
- $k_{\beta T}$ the Boltzmann constant
- T is the absolute temperature

Φ_{GB} the potential barrier height at the grain boundary
 e is the elementary charge
 l is the free path of the carriers
 w_{GB} the width of the grain boundary

Details about the model and codes are shown in the supplementary data. This model is significant because it models the weighted mobility μ_w of charge carriers in a material, considering the effects of grain boundaries.

1. $n\sigma$ term represents the product of the charge carrier concentration (n) and the electrical conductivity σ . High values typically contribute to better thermoelectric performance.
2. $\left(\frac{m_*}{m_e}\right)^{3/2}$ includes the effective mass of the charge carriers m_* , with m_e being the electron rest mass. The effective mass is related to the band structure of the material and affects how charge carriers respond to thermal energy. Higher effective masses can enhance the Seebeck coefficient but might reduce mobility.
3. $\text{Exp}\left(-\frac{k_{BT}\Phi_{GB}}{e}\right)$ is an exponential term that considers the potential barrier height at the grain boundary Φ_{GB} with k_{BT} as Boltzmann's constant, T is the absolute temperature, and e is the elementary charge. This term describes the thermionic emission effect, where charge carriers can be thermally excited over the potential barrier at the grain boundary. The higher the barrier (Φ_{GB}) the more difficult it is for carriers to cross, reducing mobility.
4. $\left(1 - \frac{l}{w_{GB}}\right)$ considers the mean free path of the carriers (l) and the width of the grain boundary w_{GB} . It implies that as the mean free path approaches the grain boundary width, the influence of the grain boundaries on charge carrier scattering becomes more pronounced.

By including terms for the potential barrier and grain boundary width, the equation accounts for the two primary ways grain boundaries impact charge transport: scattering and potential barrier resistance. The model was evaluated with the parameters selected based on an extensive review of existing data literature in the field of thermoelectric materials. From the selected studies, data, effective mass, potential barrier height, mean free path and grain boundary width were extracted. The ranges for these parameters were established based on the consensus or most frequently reported values, ensuring realistic bounds for simulations as shown in Table 1. A Python-based computational framework was developed to simulate the effects of varying parameters on mobility. The libraries and tools for the computation include NumPy For numerical operations, Matplotlib for plotting the graphs, and SciPy for more complex mathematical functions and models.

Table 1: Ranges of parameters established based on most frequently reported values 2,4,6–10,12–15,36–39

Parameter	Range
n	1×10^{17} to $5 \times 10^{18} \text{ cm}^{-3}$
m_*	$0.8 \times m_e$ to $1.2 \times m_e$
Φ_{GB}	0.1 eV to 0.5 eV
l	55 nm to 25 nm
w_G	22 nm to 10 nm

3.1. Optimizing potential barrier height (Φ_{GB})

The reduction of potential barrier height at grain boundaries within ZnO significantly enhances electron mobility as shown in Fig. 2 (a). It shows the trend where lowering the potential barrier from 0.5 eV to 0.1 eV results in an approximate 45% increase in weighted mobility. This improvement could contribute to significantly increasing the material quality factor or power factor. As Φ_{GB} decreases, the energy required for electrons to move across the boundaries also decreases, thus facilitating easier carrier movement and leading to higher mobility⁴⁸. At $\Phi_{GB}=0.5$, the mobility is at its lowest, indicating that the high energy barrier significantly hinders

electron movement. However, reducing Φ_{GB} to 0.1 results in a substantial increase in mobility which quantitatively supports the hypothesis that lower barriers enhance carrier transport⁴⁹.

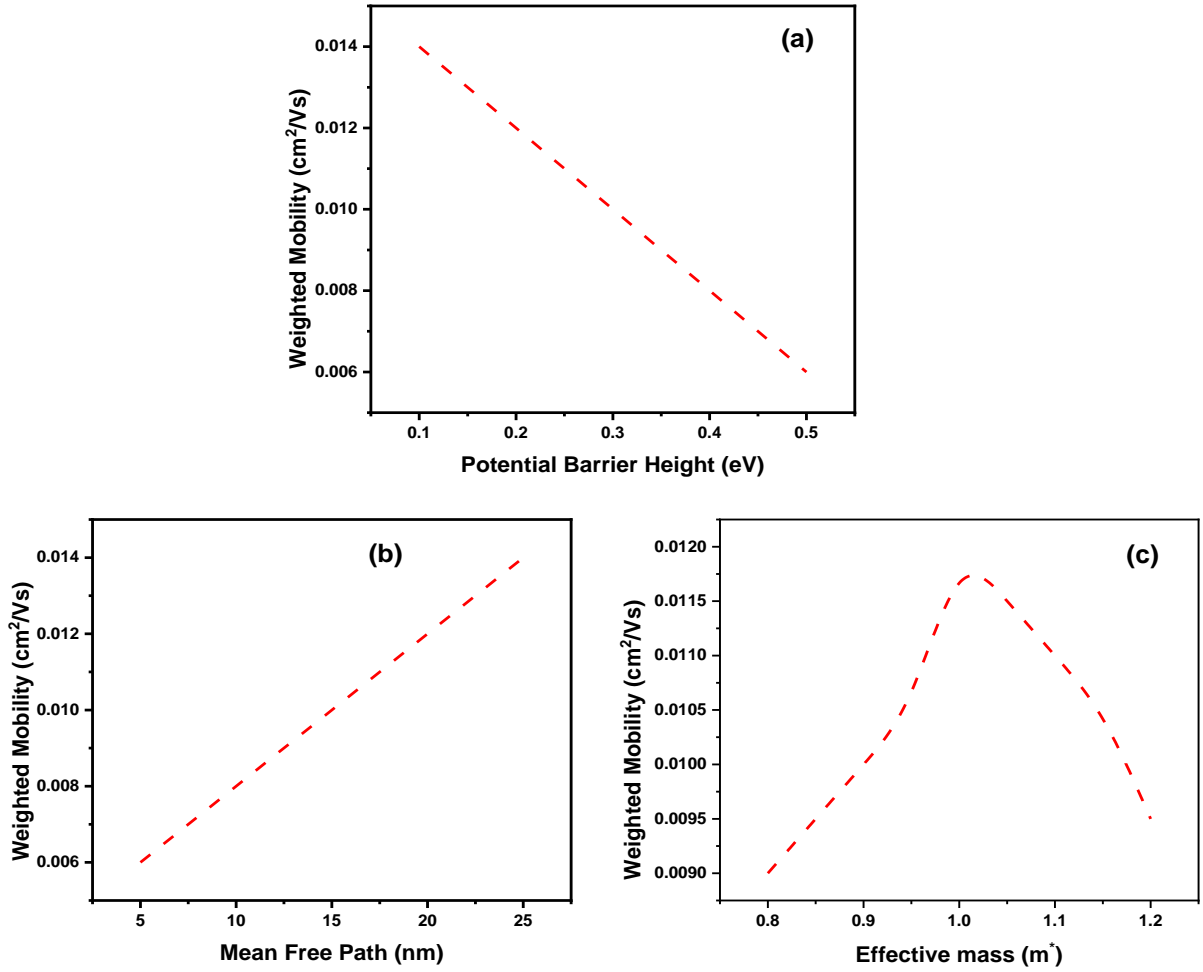


Figure 2 Optimization of Grain boundaries properties and parameters (a) Potential barrier height (b) Mean free path (c) Effective mass

These defect states can trap charge carriers, leading to a decrease in mobility which is evident from these findings as the highest mobility is achieved when the potential barrier is at its lowest (0.1 eV). Empirical studies, such as those by ⁵⁰ have shown that carrier doping, which influences the electric properties by building up potential barriers, affects the transport of the majority of carriers⁵¹. This is consistent with the observed trend in this work where a decrease in the potential barrier height correlates with enhanced mobility. Further supporting evidence comes from previous work ⁵², who highlight the significant role of energy barriers at grain boundaries in organic semiconductors. Although the material system is different, the fundamental concept of barrier influence on charge transport remains relevant. The concept of grain boundary engineering, as supported by ⁵¹ emphasizes that grain boundaries can act as traps or barriers for charge carriers in polycrystalline materials. This concept supports the findings by indicating that modifications in the grain boundary characteristics (like reducing the potential barrier height) could lead to improved electronic thermoelectric properties. This is crucial for drawing a clear connection between theoretical predictions and simulated results.

3.2. Optimizing mean free path (l)

Fig. 2b shows the positive correlation between the mean free path (l) of charge carriers and their electron mobility in semiconductor materials. The data presented show a linear increase in mobility as the mean free path extends from 5 nm to 25 nm. This observed trend is consistent with the predictions of semiclassical theory, which posits that longer mean free paths indicate fewer scattering events per unit time, thereby allowing carriers to maintain higher velocities over extended distances⁵³. The mean free path represents the average distance a charge carrier travels between collisions that affect its trajectory⁵⁴. According to the classical Drude model of electrical conductivity (3):

$$\mu = \frac{e\tau}{m^*} \quad (3)$$

where:

μ is the carrier mobility,

e is the elementary charge,

τ is the mean free time between collisions,

m^* is the effective mass of the charge carriers.

The mean free time τ can be related to the mean free path (l) by $\tau = \frac{l}{v_{th}}$, where v_{th} is the thermal velocity of the carriers. Thus, an increase in the mean free path directly enhances mobility, assuming the carrier velocity and effective mass are constant. At a shorter mean free path of 5 nm, the weighted mobility is at its minimum, highlighting the impact of frequent scattering events in significantly hindering the motion of charge carriers. As the mean free path increases to 25 nm, the number of scattering events decreases, thereby reducing the obstacles that impede carrier movement. This reduction in scattering events allows carriers to travel longer distances without deflection, increasing mobility. The findings show the potential of microstructural modifications to enhance semiconductor performance. Techniques aimed at increasing the mean free path, such as reducing impurity concentrations or defects that act as scattering centers, can effectively improve the material's electrical conductivity. This concept is further supported by 55,56 which highlighted the impact of grain boundaries on carrier mobility by reducing the mean free path through scattering events. Furthermore, studies by 37,57 demonstrated that grain boundaries could significantly reduce the mean free path of phonons, affecting thermal conductivity in materials. The scattering of phonons at grain boundaries leads to a decrease in the mean free path of heat-carrying vibrations, resulting in lower thermal conductivity. Additionally, research by 58,59 has shown that grain boundaries contribute to phonon scattering and thermal resistance, leading to a decrease in the average mean free path of phonons. This phenomenon is crucial for understanding heat conduction mechanisms in polycrystalline materials, where grain boundaries act as barriers to phonon transport.

3.3. Effective mass optimization

Figure 2c shows a parabolic relationship between the effective mass of charge carriers in ZnO and their mobility. It is shown that as the effective mass increases from 0.8 m_e to 1.0 m_e , electron mobility increases, peaking at 1.0 m_e . This peak suggests an optimal balance of effective mass where electron mobility is maximized, implying an intricate interplay between carrier mass and lattice interaction forces within the material. The effective mass is a fundamental parameter in semiconductor physics that reflects the inertia a charge carrier exhibits when subjected to electric fields, thereby influencing how the band structure affects carrier dynamics^{60,61}. The observed parabolic trend in carrier mobility with varying effective mass indicates that there exists an optimal carrier mass for maximum mobility. This optimal point likely represents a critical balance between the effective mass and associated scattering mechanisms within ZnO. The effective mass is influenced by the curvature of the conduction and valence bands, as outlined by the Kane model and the k·p theory^{62,63}. A lower effective mass typically indicates a higher curvature of these bands, suggesting that the bands are more dispersed. This dispersion generally facilitates higher mobility due to fewer collisions with lattice imperfections⁶². Doping ZnO with elements like aluminum (Al) can reduce the effective mass by altering the band structure, enhancing mobility up to a certain doping level^{12,36}. This is consistent with the trends observed, where mobility increases with a reduction in effective mass up to the electron mass, beyond which increased defect scattering due to

further increases in effective mass leads to a decrease in mobility. When the effective mass exceeds the actual electron mass ($1.0 m_e$) there is a noticeable decrease in mobility. This reduction is attributed to increased scattering with defects or phonons, which becomes more significant as the effective mass increases, effectively slowing down the carriers. Furthermore, optimizing the effective mass could contribute to improvements in the Seebeck coefficient and material quality factor (B), as the effective mass directly influences it.

4. Strategies for the development of efficient ZnO materials

The research and model development outcomes provide a solid foundation for novel experimental strategies aimed at enhancing the ZT of ZnO for thermoelectric applications. These strategies can focus on manipulating intrinsic material properties at the micro and nano scales, specifically targeting the reduction of potential barrier heights, optimizing carrier concentrations through sophisticated doping mechanisms, and engineering microstructural dimensions to improve electron mobility and reduce thermal conductivity.

4.1. Microstructural Engineering

Current research in thermoelectric materials frequently employs nanostructuring techniques to alter phonon transport and enhance electron mobility. This method involves the strategic incorporation of nanoparticles and the formation of disordered lattice structures, which effectively scatter phonons, thereby reducing K_L . In ZnO, further enhancements can be achieved through meticulous control over the powder or grain size, shape, and the deliberate distribution and orientation of grain boundaries. Such precision engineering facilitates optimized electron flow and significantly minimizes phonon transport. Beyond traditional nanostructuring, the integration of two-dimensional (2D) materials such as graphene into the ZnO matrix marks a considerable advancement²⁷. These 2D materials act as barriers that effectively modulate phonon scattering without significantly affecting the mobility of charge carriers. When this strategy is paired with optimized sintering techniques, the resultant effect could not only be an enhancement in electrical conductivity but also a more substantial reduction in thermal conductivity compared to nanostructuring alone. The use of materials like SiC or TiO₂ nanoparticles at grain boundaries is a further innovation in this field^{65,66}. These nanoparticles serve as precise scattering centers for phonons, strategically exploiting the differences in phonon and electron mean-free paths to selectively scatter phonons while preserving electron transport. This approach has demonstrated considerable success in Bi₂Te₃ thermoelectrics, notably reducing lattice K_L while maintaining electrical properties, as documented by³⁸. Applying these nano-structuring techniques to use the wurtzite structure of ZnO may lead to a more profound decrease in K_L , potentially outperforming traditional methods utilized in materials such as SrTiO₃. This methodical and innovative approach not only refines existing practices but also establishes new standards in the design and development of high-efficiency thermoelectric materials.

The performance outlook of materials, when thermal conductivity (K_L) is optimized through microstructural engineering, can be evaluated by analyzing the quality factor (B). Previous research indicates that the K_L of SrTiO₃ can be reduced to as low as 1.2 W/mK at room temperature when the grain size of 24 nm is achieved through nanostructuring and this value is unlikely to decrease further below approximately 1 W/mK due to the diffusive limit¹⁷. Building on this insight, an analysis was performed on ZnO materials to explore the performance outlook of ZnO when K_L is optimized through microstructural engineering. This investigation is critical as it illustrates how grain size modifications and K_L optimization can improve material efficiencies. The B factor was calculated using Equation (4), which incorporated the weighted mobility for polycrystal 1, as shown in Figure 1(d).

$$B = 9 \frac{\mu_W}{K_L} \left(\frac{T}{300} \right)^{5/2} \quad (4)$$

Where μ_W is the weighted mobility having unit's $\text{cm}^2\text{V}^{-1}\text{s}^{-1}$, K_L is lattice thermal conductivity and T is the absolute temperature. Figure 3 shows the predicted quality factor B across a range of temperatures. The observed trend of increasing B with decreasing K_L from 7 to 1 W/mK shows the crucial role of reduced thermal conductivity K_L in enhancing the performance of ZnO. This trend indicates that by predominantly influencing phonon scattering at grain boundaries across the entire temperature spectrum, improvements in ZnO's performance can be achieved. This prediction implies that a reduction in K_L could facilitate the development of

efficient ZnO materials tailored for low-temperature thermoelectric applications. Consequently, this analysis provides valuable insights into the potential impact of nanostructuring engineering, suggesting it could serve as a pathway in the advancement of efficient ZnO thermoelectric materials.

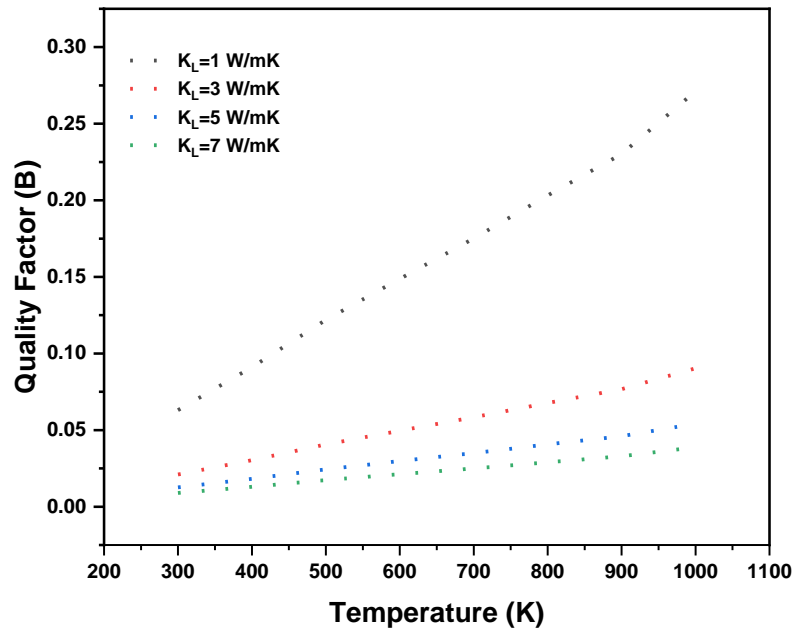


Figure 3 Calculated Quality Factor for Polycrystalline sample (Polycrystal 1 in Figure 2)

4.2. Single and Dual Element Doping Strategies

4.2.1. Single-Element Doping

Traditional doping practices often utilize elements such as aluminum (Al), gallium (Ga), or indium (In) to increase carrier concentration and modify thermal and electrical conductivity⁹. For instance, doping ZnO with Al has been shown to increase free electron concentration substantially, thereby reducing resistivity and enhancing electrical properties¹⁴. The strategic focus of future work should involve fine-tuning the type and concentration of such dopants to maximize electrical conductivity while minimizing carrier scattering, thus achieving an optimal balance for improved thermoelectric properties.

4.2.2. Dual Element Doping

Building upon the foundation of single-element doping, dual doping involves using combinations of elements that can synergistically alter the electronic and thermal properties of ZnO more effectively. This strategy utilizes elements that can exist in multiple valence states, such as cerium (Ce), which can dynamically adjust the charge carrier concentration and mobility depending on the operational environment. Additionally, designing specific defect configurations at grain boundaries can collectively alter the electronic structure to reduce energy barriers and enhance carrier mobility, going beyond traditional doping to create targeted modifications that optimize both conductivity and the Seebeck coefficient. Table 2 outlines potential dual-doping combinations, their stoichiometries, and their expected impacts on ZnO's thermoelectric properties.

Table 2: Dopant Combinations and Stoichiometries

Base Material	Dopant 1	Dopant 2	Chemical Equation	Description
ZnO	Cu	Ce	$Zn_{1-x-y}Cu_xCe_yO$	Cu and Ce co-doping; Cu enhances electrical conductivity; Ce allows dynamic charge carrier management through its variable valence states.
ZnO	Al	Bi	$Zn_{1-x-y}Al_xBi_yO$	Al and Bi co-doping; Al increases carrier concentration, Bi reduces thermal conductivity due to its heavy mass, and increases the Seebeck coefficient.
ZnO	Ag	Ga	$Zn_{1-x-y}Ag_xGa_yO$	Ag and Ga co-doping; Ag boosts conductivity, and Ga enhances carrier mobility by modifying band structure.
ZnO	Cu	Ga	$Zn_{1-x-y}Cu_xGa_yO$	Cu and Ga co-doping; balances Cu's conductive properties with Ga's ability to modulate carrier mobility.
ZnO	Ce	Bi	$Zn_{1-x-y}Ce_xBi_yO$	Ce and Bi co-doping; combines Ce's variable valence states with Bi's impact on thermal and electronic transport

4.2.3. Passivation of Grain Boundaries

The strategy of passivating grain boundaries using compounds that form strong bonds with ZnO, such as phosphates or borates, targets reducing potential barriers and enhancing electron mobility by neutralizing defect states at the grain boundaries^{70,71}. Similar strategies have proven effective in semiconductor devices, such as in Si solar cells where SiNx passivation improved carrier lifetime and efficiency (Schroder, Semiconductor Material and Device Characterization)⁷¹. For ZnO, optimizing the choice and method of deposition of passivating agents could significantly enhance its thermoelectric performance by mitigating the adverse effects of native defects.

5. Conclusion

This study advances our understanding of the thermoelectric properties of Zinc Oxide (ZnO) and demonstrates the feasibility of improving its quality factor through strategic grain boundary engineering. By integrating a comprehensive model with Python-based computational simulations, the research elucidates the profound impact of grain boundary parameters on charge carrier dynamics, thereby uncovering methods to enhance electron mobility and reduce energy barriers. The empirical data derived from these simulations suggest that optimizing parameters such as barrier height, the electron mean free path and effective mass can lead to a substantial increase in the thermoelectric performance of ZnO materials. Moreover, the findings of this study provide actionable insights into the application of advanced material engineering techniques, such as dual doping and the integration of graphene layers, which have shown promise in reducing thermal conductivity without compromising the integrity of charge transport. These strategies, alongside the demonstrated ability to fine-tune microstructural properties, offer a robust pathway toward significantly enhancing the energy conversion efficiency of ZnO-based thermoelectric materials. This research not only contributes a novel framework for grain boundary engineering but also lays the groundwork for future empirical investigations aimed at validating and refining the proposed models. The potential transformation of ZnO into a more effective thermoelectric material could have substantial implications for the development of sustainable energy technologies, marking a crucial step toward the realization of high-performance thermoelectric systems. The continuation of this work is crucial for moving from theoretical models to practical applications, thereby

advancing the field of materials science toward achieving more efficient thermoelectric materials for global energy solutions.

References

- 1 J. Zhang, L. Song, G. K. H. Madsen, K. F. Fischer, W. Zhang, X. Shi and B. B. Iversen, *Nat Commun*, DOI:10.1038/ncomms10892.
- 2 D. B. Zhang, H. Z. Li, B. P. Zhang, D. D. Liang and M. Xia, *RSC Adv*, 2017, **7**, 10855–10864.
- 3 X. Tao, J. Dutson, C. Zeng, C. Asker, S. Luong, A. Reza, B. Hao, Z. Zhang, J. Ellingford, R. S. Bonilla, O. Fenwick, E. Bilotti, F. Hofmann, M. Thwaites and H. E. Assender, *Adv Mater Technol*, , DOI:10.1002/admt.202301958.
- 4 T. Koskinen, U. Volin, C. Tossi, R. Ramesh and Ii. Tittonen, *Nanotechnology*, DOI:10.1088/1361-6528/ac9980.
- 5 C. Peng, L. Zhang, G. Zhang, C. Wang, Y. Yan, Y. Wang and M. Hu, *J Phys D Appl Phys*, DOI:10.1088/1361-6463/aacf19.
- 6 M. Ohtaki, K. Araki and K. Yamamoto, *J Electron Mater*, DOI:10.1007/s11664-009-0816-1.
- 7 S. Y. Bae, C. W. Na, J. H. Kang and J. Park, *J Phys Chem B*, , DOI:10.1021/jp0458708.
- 8 X. Liang, *J Eur Ceram Soc*, , DOI:10.1016/j.jeurceramsoc.2016.02.017.
- 9 P. Jood, R. J. Mehta, Y. Zhang, T. Borca-Tasciuc, S. X. Dou, D. J. Singh and G. Ramanath, *RSC Adv*, DOI:10.1039/c3ra46813e.
- 10 N. H. T. Nguyen, T. H. Nguyen, Y. Liu, M. Aminzare, A. T. Phạm, S. Cho, D. Wong, K. Chen, T. Seetawan, N. K. Pham, H. K. T. Ta, V. C. Trần and T. B. Phan, *ACS Appl Mater Interfaces*, DOI:10.1021/acsami.6b10591.
- 11 S. Acharya, B.-K. Yu, J. Hwang, J. Kim and W. Kim, *Adv Funct Mater*, DOI:10.1002/adfm.202105008.
- 12 P. Sikam, P. Moontragoon, Z. Ikonić, T. Kaewmaraya and P. Thongbai, *Appl Surf Sci*, DOI:10.1016/j.apsusc.2019.02.255.
- 13 D. C. Truong, A. T. Phạm, O. K. T. Le, D. Van Hoang, T. H. Nguyen, H. K. T. Ta, N. K. Pham, H. T. Lai, T. B. Phan and V. C. Trần, *Science and Technology Development Journal*, DOI:10.32508/stdj.v23i4.2458.
- 14 B. Park, *The Journal of Physical Chemistry C*, DOI:10.1021/acs.jpcc.3c07518.
- 15 H. T. Wu, Y. C. Su, C. Pao and C. Shih, *ACS Appl Mater Interfaces*, DOI:10.1021/acsami.8b20725.
- 16 W. Y. Lim, D. Zhang, S. S. F. Duran, X. Y. Tan, C. K. I. Tan, J. Xu and A. Suwardi, *Front Phys*, DOI:10.3389/fphy.2021.755597.

- 17 M. Dylla, J. J. Kuo, I. T. Witting and G. J. Snyder, *Adv Mater Interfaces*, DOI:10.1002/admi.201900222.
- 18 C. Zhang, X. Geng, B. Chen, J. Li, A. Meledin, L. Hu, F. Liu, J. Shi, J. Mayer, M. Wuttig, O. Cojocar-Mirédin and Y. Yu, *Small*, , DOI:10.1002/sml.202104067.
- 19 L. Wang, H. Liu and L. Xing, *Micromachines (Basel)*, DOI:10.3390/mi13050743.
- 20 J. E. Halpin, B. M. Jenkins, M. P. Moody, R. W. H. Webster, J. G. Bos, P. A. J. Bagot and D. A. MacLaren, *ACS Appl Electron Mater*, DOI:10.1021/acsaelm.2c00699.
- 21 A. P. Zavjalov, S. A. Tikhonov and D. Yu. Kosyanov, *Materials*, , DOI:10.3390/ma12182895.
- 22 J. Cao, D. Ekren, Y. Peng, F. Azough, I. A. Kinloch and R. Freer, *ACS Appl Mater Interfaces*, DOI:10.1021/acsaemi.0c21699.
- 23 T. Horide, Y. Murakami, M. Ishimaru and K. Matsumoto, *ACS Appl Electron Mater*, DOI:10.1021/acsaelm.2c01486.
- 24 Y. Pan, U. Aydemir, J. A. Grovogui, I. T. Witting, R. Hanus, Y. Xu, J. Wu, C. Wu, F. Sun, H. Zhuang, J. Dong, J. Li, V. P. Dravid, and G. J. Snyder, *Advanced Materials*, DOI:10.1002/adma.201802016.
- 25 J. Martin, L. Wang, L. Chen and G. S. Nolas, *Phys Rev B*, DOI:10.1103/physrevb.79.115311.
- 26 H. Kim, Z. Wang, M. N. Hedhili, N. Wehbe and H. N. Alshareef, *Chemistry of Materials*, DOI:10.1021/acs.chemmater.6b04654.
- 27 M. Choi, J. An, H. Lee, H. Jang, J. H. Park, D. Cho, J. Y. Song, S. M. Kim, M.-W. Oh, H. Shin and S. Jeon, *Nat Commun*, DOI:10.1038/s41467-024-46182-2.
- 28 W. H. Nam, Y. S. Lim, S. C. Choi, W. Seo and J. Y. Lee, *J Mater Chem*, 2012, **22**, 14633.
- 29 T. Watanabe, H. Yoshida, Y. Ikuhara, T. Sakuma, H. Muto and M. Sakai, *Mater Trans*, 2002, **43**, 1561–1565.
- 30 V. A. Borovikov, M. I. Mendeleev and A. H. King, *Int J Plast*, 2018, **109**, 79–87.
- 31 X. Li, Z. Yao, J. Xie, Z. Li, H. Hao, M. Cao, A. Ullah, A. Ullah, A. Manan and H. Liu, *J Adv Dielectr*, 2018, **08**, 1850044.
- 32 S. B. Carter and A. M. Hodge, DOI:10.2172/929157.
- 33 G. Soye, J. A. Eastman, L. J. Thompson, G. R. Bai, P. M. Baldo, A. W. McCormick, R. J. DiMelfi, A. A. Elmustafa, M. F. Tambwe and D. S. Stone, *Appl Phys Lett*, 2000, **77**, 1155–1157.
- 34 X. Guo and J. Maier, *J Electrochem Soc*, 2001, **148**, E121.
- 35 M. A. Atwater, R. O. Scattergood and C. C. Koch, *Materials Science and Engineering A*, 2013, **559**, 250–256.
- 36 D. Nie, T. Xue and X. Li, *Sci China B Chem*, , DOI:10.1007/s11426-008-0061-0.

- 37 Z. L. Wang, *Journal of Physics Condensed Matter*, DOI:10.1088/0953-8984/16/25/r01.
- 38 K. H. Kim, S. Shim, K. B. Shim, K. Niihara and J. Hojo, *Journal of the American Ceramic Society*, DOI:10.1111/j.1551-2916.2005.00131.x.
- 39 S. Acharya, B.-K. Yu, J. Hwang, J. Kim and W. Kim, *Adv Funct Mater*, DOI:10.1002/adfm.202105008.
- 40 D. Bilc, G. Hautier, D. Waroquiers, G. Rignanese and P. Ghosez, *Phys Rev Lett*, , DOI:10.1103/physrevlett.114.136601.
- 41 J. Qin, Y. Yang, L. Wang, H. Sun, Y. T. Liu, C. Ke, C. H. Cheng and Y. Zhao, *J Supercond Nov Magn*, DOI:10.1007/s10948-021-06096-2.
- 42 R. Hanus, M. T. Agne, A. J. E. Rettie, Z. Chen, G. Tan, D. Y. Chung, M. G. Kanatzidis, Y. Pei, P. W. Voorhees and G. J. Snyder, *Advanced Materials*, DOI:10.1002/adma.201900108.
- 43 Z. Chu, M. Yang, P. Schulz, D. Wu, X. Ma, E. Seifert, L. Sun, X. Li, K. Zhu and K. Lai, *Nat Commun*, , DOI:10.1038/s41467-017-02331-4.
- 44 O. K. Truong Le, A. T. Thanh Pham, N. K. Pham, T. H. Cao Pham, T. H. Nguyen, D. Van Hoang, H. K. Thi Ta, D. C. Truong, H. T. Lai, T. D. Thi Ung, V. C. Tran and T. B. Phan, *Journal of Materiomics*, 2021, **7**, 742–755.
- 45 S. Sulaiman, S. Izman, M. B. Uday and M. F. Omar, *RSC Adv*, 2022, **12**, 5428–5438.
- 46 W. H. Nam, B. B. Kim, Y. S. Lim, K. S. Dae, W.-S. Seo, H.-H. Park and J. Y. Lee, *Nanoscale*, 2017, **9**, 12941–12948.
- 47 K. H. Kim, S. Shim, K. B. Shim, K. Niihara and J. Hojo, *Journal of the American Ceramic Society*, 2005, **88**, 628–632.
- 48 R. F. Schmitsdorf, T. U. Kampen and W. Mönch, *Journal of Vacuum Science & Technology B Microelectronics and Nanometer Structures Processing Measurement and Phenomena*, DOI:10.1116/1.589442.
- 49 P. Dixit, S. S. Jana and T. Maiti, *Small*, , DOI:10.1002/sml.202206710.
- 50 M. Kimura, R. Nozawa, S. Inoue, T. Shimoda, B. O.-K. Lui, S. W.-B. Tam and P. Migliorato, *Jpn J Appl Phys*, , DOI:10.1143/jjap.40.5227.
- 51 T. Meier, H. Bäßler and A. Köhler, *Adv Opt Mater*, , DOI:10.1002/adom.202100115.
- 52 I. Vladimirov, M. Kühn, T. Geßner, F. May and R. T. Weitz, *Sci Rep*, , DOI:10.1038/s41598-018-33308-y.
- 53 Y. Tan, Y. Zhang, K. I. Bolotin, Y. Zhao, S. Adam, E. H. Hwang, S. Das Sarma, H. L. Störmer and P. Kim, *Phys Rev Lett*, , DOI:10.1103/physrevlett.99.246803.
- 54 S. Sharma, A. Khandelwal, E. P. Amaladass, S. Abhirami, Sk. Ramjan, J. Jayabalan, A. Mani and M. K. Chattopadhyay, *J Appl Phys*, DOI:10.1063/5.0013939.

- 55 A. J. Minnich, M. S. Dresselhaus, Z. Ren and G. Chen, *Energy Environ Sci*, , DOI:10.1039/b822664b.
- 56 D. G. Cahill, W. K. Ford, K. E. Goodson, G. D. Mahan, A. Majumdar, H. J. Maris, R. Merlin and S. R. Phillpot, *J Appl Phys*, DOI:10.1063/1.1524305.
- 57 J. W. Lawson, M. S. Daw, T. H. Squire and C. W. Bauschlicher, *Journal of the American Ceramic Society*, DOI:10.1111/jace.12037.
- 58 P. S. De and R. S. Mishra, *Metallurgical and Materials Transactions A*, DOI:10.1007/s11661-011-0912-8.
- 59 P. G. Klemens, *Int J Thermophys*, , DOI:10.1007/bf01458842.
- 60 A. Parveen and G. Vaitheeswaran, *Sci Rep*, , DOI:10.1038/s41598-018-31300-0.
- 61 T. M. Brenner, D. Egger, A. M. Rappe, L. Kronik, G. Hodes and D. Cahen, *J Phys Chem Lett*, , DOI:10.1021/acs.jpcclett.5b02390.
- 62 M. Dendzik, M. Michiardi, C. E. Sanders, M. Bianchi, J. A. Miwa, S. S. Grønberg, J. V Lauritsen, A. Bruix, B. Hammer and P. Hofmann, *Phys Rev B*, , DOI:10.1103/physrevb.92.245442.
- 63 C. Segarra, J. Planelles and S. E. Ulloa, *Phys Rev B*, , DOI:10.1103/physrevb.93.085312.
- 64 C. Zhou, Y. K. Lee, J. Cha, B. Yoo, S. Cho, T. Hyeon and I. J. Chung, *J Am Chem Soc*, DOI:10.1021/jacs.8b05741.
- 65 P. Liu, P. Yao and J. Liu, *J Electron Mater*, 2008, **37**, 874–879.
- 66 X. Sun, J. Li, S. Guo, Z. Xiu, K. Duan and X. Hu, *Journal of the American Ceramic Society*, 2005, **88**, 1536–1543.
- 67 J. Y. Wang, Y. Lin, C.-W. Wu, C. Y. Chiu, C. H. Lee, C. Y. Yeh, B. Huang and C. Y. Liu, *Journal of the American Ceramic Society*, 2020, **104**, 1707–1715.
- 68 A. Janotti and C. G. Van de Walle, *Reports on Progress in Physics*, 2009, **72**, 126501.